Journal of Dental Research
DS1–DS8

DOI: 10.1177/0022034516640246
jdr.sagepub.com

# Role of PHOSPHO1 in Periodontal Development and Function

**L.E. Zweifler[1], M. Ao[2], M. Yadav[3], P. Kuss[3], S. Narisawa[3], T.N. Kolli[1], H.F. Wimer[4,5], C. Farquharson[6], M.J. Somerman[2], J.L. Millán[3], and B.L. Foster[1]**

## Appendix

### *Materials and Methods*

*Genotyping.* Colonies of *Phospho1* and *Spp* mice (both on a C57BL/6 background) were maintained by heterozygote breeding to generate wild-type (WT) controls and homozygous knockout mice, while *Phospho1*$^{-/-}$; *Spp1*$^{-/-}$ double knockout mice were prepared by double heterozygote breeding, as described previously (Yadav et al. 2014). Genotyping was performed by polymerase chain reaction and agarose gel electrophoresis. Primers for *Phospho1* mouse genotyping were as follows: TCCTCCTCACCTTCGACTTC-3 (forward) and ATGCGGCGGAATAAACTGT (reverse). The 355-bp amplicon from *Phospho1* exon 2 was incubated with BsrDI restriction enzyme to identify the intact 355-bp WT band or digested 144-bp and 211-bp fragments due to a point mutation in *Phospho1*$^{-/-}$ mice (Appendix Fig. 1A). Primers for *Spp1* mouse genotyping were as follows: AGAGGTGAGGTCCTCATCTGTGGCA (forward) and ACTCCAATCGTCCCTACAGTCGATGTC (reverse). Primers for *Spp1* amplified an 821-bp product in WT and a 1.8-kb product in *Spp*$^{-/-}$ mice (Appendix Fig. 1B).

*Quantitative micro–computed tomography.* For quantitative micro–computed tomography analysis, hemi-mandibles at 30 d postnatal (dpn) ($n = 5$ per genotype) were scanned in 70% ethanol on a Scanco μCT 35 (Scanco Medical) with the following parameters: 15 μm voxel size, 55 KVp, and 145 mA, with a 0.36° rotation step (180° angular range) and 400-ms exposure per view. Scans were calibrated to a set of hydroxyapatite (HA) phantom standards provided by the manufacturer. Scanco μCT software (HP, DECwindows Motif 1.6) was used for 3-dimensional (3D) reconstruction and image viewing. After 3D reconstruction, volumes of enamel, crown dentin, root dentin, and alveolar bone were contoured and segmented using a global threshold of 0.6 g HA/cm$^3$. Tissue volume (TV), bone volume (BV), bone volume fraction (BV/TV), bone thickness, and tissue mineral density were calculated.

*Histomorphometry.* For comparison of WT and *Phospho1*$^{-/-}$ mouse dentoalveolar tissues, serial coronal (buccal-lingual) sections were prepared from paraffin-embedded hemi-mandibles. Central sections of the mesial first molar root were selected for measurement. Histomorphometry was performed on hematoxylin and eosin (H&E)–stained sections using a slide scanner (Leica SCN400F) with Digital Imaging Hub software (Leica Microsystems). Predentin, dentin, mantle dentin, acellular cementum, periodontal ligament, and alveolar bone width were measured on lingual and buccal aspects of the first mandibular molar mesial root at a distance of 300 μm from the cementoenamel junction (CEJ) in 14-, 30-, and 90-d postnatal (dpn) WT and *Phospho1*$^{-/-}$ mice. Additional measurements included the CEJ–alveolar bone crest (ABC) at 30 and 90 dpn, dentin mineralization lag (tip of new dentin matrix to the mineralization front, as judged by H&E staining) and cementum initiation distance (tip of new dentin to first deposition of acellular cementum) at 14 dpn, molar root height (CEJ to the apex) at 14 and 30 dpn, root dentin height (root height minus cellular cementum) at 14 and 30 dpn, and cellular cementum area (lingual and buccal aspects measured and combined) at 30 and 90 dpn.

### Appendix Reference

Yadav MC, Huesa C, Narisawa S, Hoylaerts MF, Moreau A, Farquharson C, Millan JL. 2014. Ablation of osteopontin improves the skeletal phenotype of phospho1 mice. J Bone Miner Res. 29(11):2369–2381.

[1]Division of Biosciences, College of Dentistry, Ohio State University, Columbus, OH, USA
[2]National Institute of Arthritis and Musculoskeletal and Skin Diseases, National Institutes of Health, Bethesda, MD, USA
[3]Sanford Children's Health Research Center, Sanford Burnham Prebys Medical Discovery Institute, La Jolla, CA, USA
[4]Department of Vertebrate Zoology, National Museum of Natural History, Smithsonian Institution, Washington, DC, USA
[5]National Institute of Dental and Craniofacial Research, National Institutes of Health, Bethesda, MD, USA
[6]Roslin Institute and Royal (Dick) School of Veterinary Studies, University of Edinburgh, Easter Bush, Midlothian, UK

**Corresponding Author:**
B.L. Foster, Division of Biosciences, College of Dentistry, Ohio State University, 305 W. 12th Avenue, 4163 Postle Hall, Columbus, OH 43210, USA.
Email: foster.1004@osu.edu

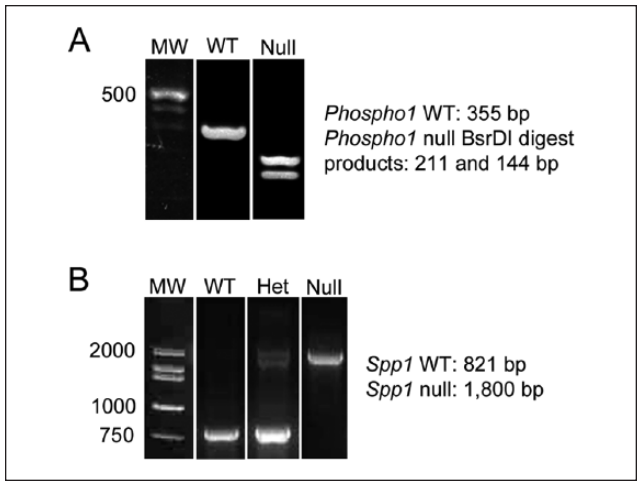


**Appendix Figure 1.** Genotyping *Phospho1* and *Spp1* mice. Polymerase chain reaction and gel electrophoresis were used for mouse genotyping. Primer sequences are provided in the Appendix Materials and Methods. (**A**) The 355 bp amplicon from *Phospho1* exon 2 was incubated with BsrDI restriction enzyme to identify the intact 355-bp wild-type (WT) band or digested 144-bp and 211-bp fragments due to a point mutation in *Phospho1*$^{-/-}$ mice. (**B**) *Spp1* mice are identified by an 821-bp product for the *Spp1*$^{+}$ WT allele, an 1,800-bp product for the *Spp1*$^{-}$ null allele, or the presence of both products in *Spp1*$^{+/-}$ heterozygote (Het) mice. MW, molecular weight marker (numbers to the left of the gel images represent MW band sizes).

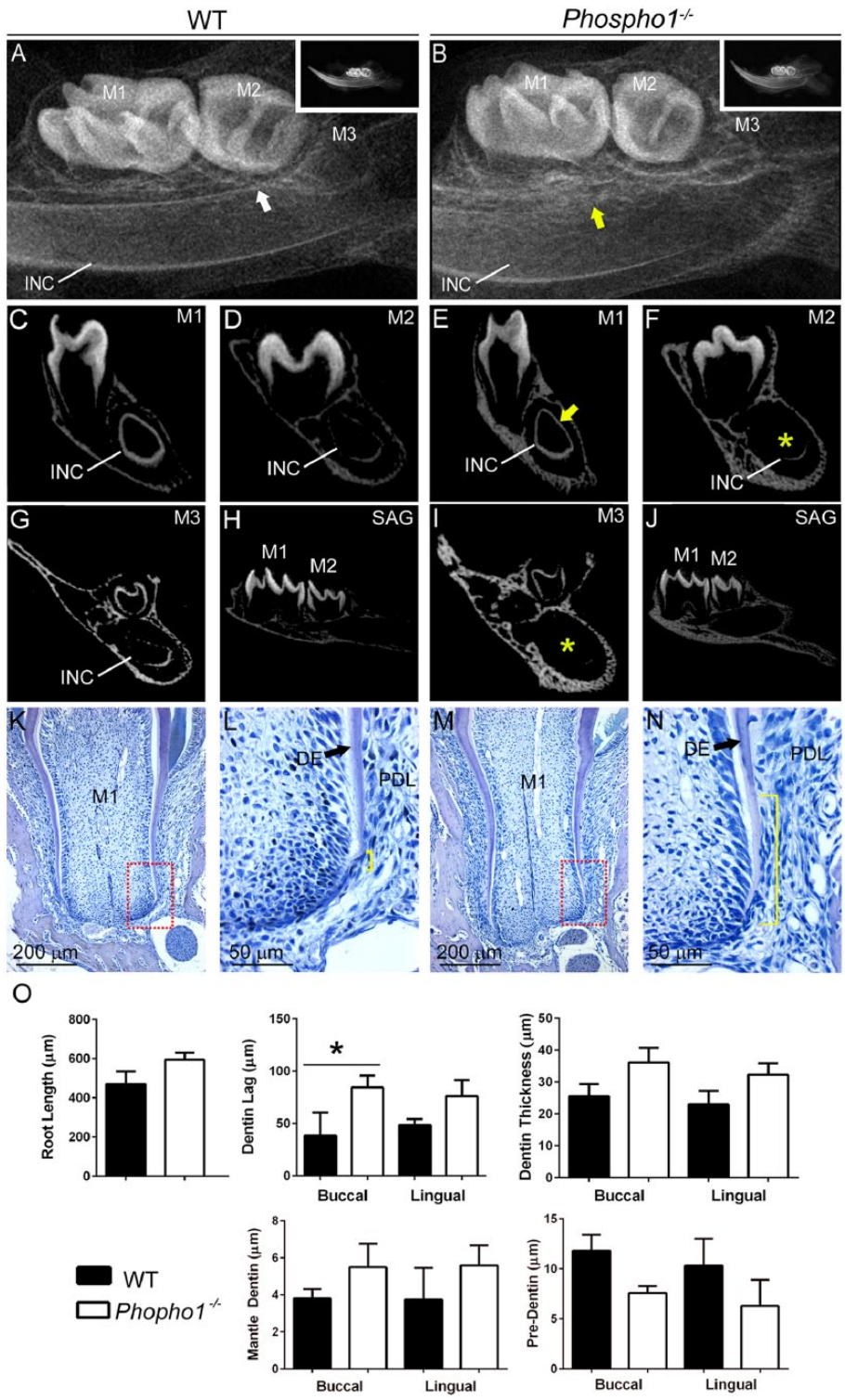


**Appendix Figure 2.** Developmental dentin defects in *Phospho1*$^{-/-}$ mice at 14 d postnatal (dpn). (**A, B**) Radiography of the mandible indicates delayed dentin (DE) mineralization of the *Phospho1*$^{-/-}$ mouse incisor (INC), where the wild-type (WT) incisor lingual (root) aspect initiates near the second molar (M2; white arrow in A) and the *Phospho1*$^{-/-}$ incisor lingual aspect initiates beneath the first molar (M1; yellow arrow in B). (**C–J**) Micro–computed tomography analysis indicates delayed DE mineralization (yellow asterisks) and thin incisor dentin (yellow arrow) in *Phospho1*$^{-/-}$ mouse incisors. (**K–N**) By histology, an apparent delay in DE mineralization is observed in the first mandibular molar in hematoxylin and eosin (H&E)–stained sections (red boxes in K and M indicate higher magnification L and N, respectively). Yellow brackets in N versus L indicate the lag between DE matrix production and mineralization, with a larger distance suggesting delayed DE mineralization in *Phospho1*$^{-/-}$ mice compared with controls. (**O**) Histomorphometry conducted on H&E-stained section confirms significantly delayed DE mineralization (*$P < 0.05$) on the buccal aspect of the first mandibular molar. Other measurements on root DE did not indicate significant differences between *Phospho1*$^{-/-}$ and control mice ($P > 0.05$) at this age. INC, incisor; M3, third molar; PDL, periodontal ligament; SAG, sagittal plane.

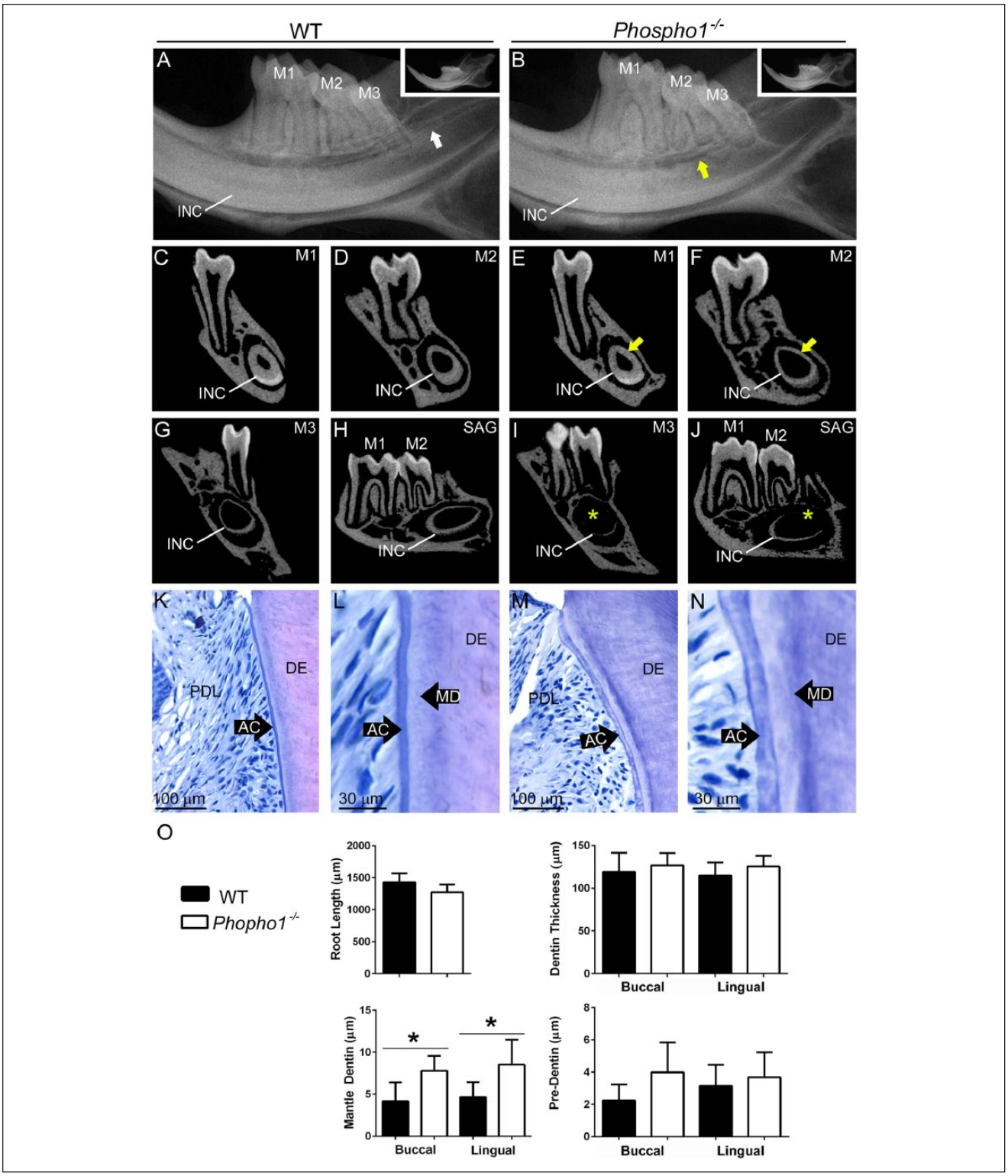


**Appendix Figure 3.** Developmental dentin defects in *Phospho1*$^{-/-}$ mice at 30 d postnatal (dpn). Radiography, micro–computed tomography (micro-CT), and histology analysis of *Phospho1*$^{-/-}$ mouse incisors and molars at 30 dpn identify similar dentin defects as are observed at 14 dpn (Appendix Fig. 2). (**A, B**) Radiography of the mandible indicates delayed dentin (DE) mineralization of the *Phospho1*$^{-/-}$ mouse incisor (INC), where the wild-type (WT) incisor lingual (root) aspect initiates well behind third molar (M3; white arrow in A) and the *Phospho1*$^{-/-}$ incisor lingual aspect initiates beneath the second molar (M2; yellow arrow in B). (**C–J**) Micro-CT analysis indicates delayed DE mineralization (yellow asterisks) and thin incisor DE (yellow arrows) in *Phospho1*$^{-/-}$ mouse incisors. (**K–N**) Histology reveals an altered mantle dentin (MD) layer of *Phospho1*$^{-/-}$ versus WT control mice, including increased width and globular appearance. (**O**) Histomorphometry conducted on hematoxylin and eosin (H&E)–stained sections confirms a significantly increased MD layer (*$P < 0.05$) in *Phospho1*$^{-/-}$ versus WT mice, whereas other DE parameters do not appear different at 30 dpn. AC, acellular cementum; M1, first molar; PDL, periodontal ligament; SAG, sagittal plane.

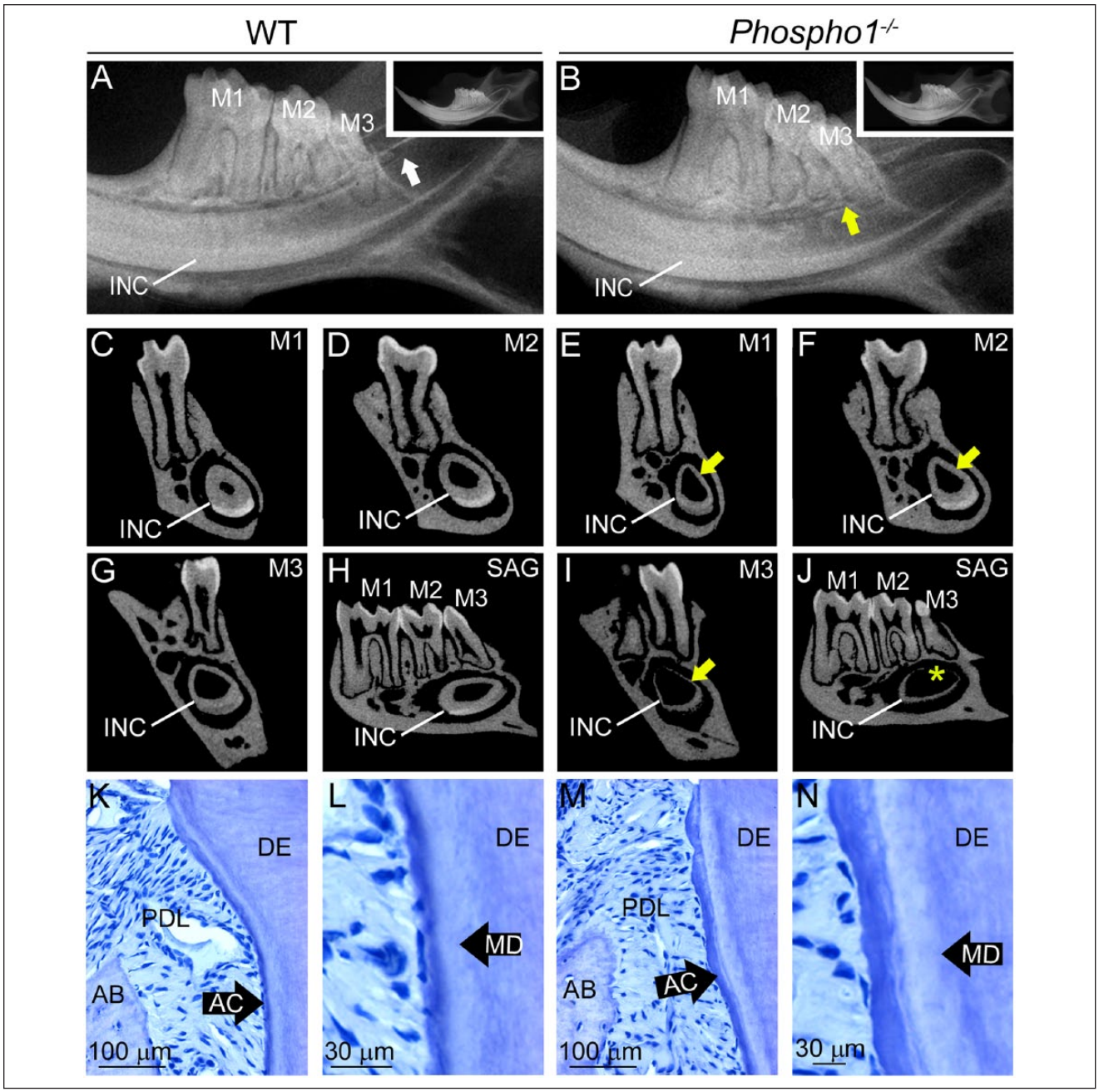


**Appendix Figure 4.** Developmental dentin defects in *Phospho1*$^{-/-}$ mice at 90 d postnatal (dpn). Radiography, micro–computed tomography (micro-CT), and histology analysis of *Phospho1*$^{-/-}$ mouse incisors and molars at 90 dpn identify similar dentin defects as are observed at 14 and 30 dpn (Appendix Figs. 2 and 3). (**A, B**) Radiography of the mandible indicates delayed dentin (DE) mineralization of the *Phospho1*$^{-/-}$ mouse incisor (INC), where the wild-type (WT) incisor lingual (root) aspect initiates well behind third molar (M3; white arrow in A) and the *Phospho1*$^{-/-}$ incisor lingual aspect initiates beneath the mesial third molar (M3; yellow arrow in B). (**C–J**) Micro-CT analysis indicates delayed DE mineralization (yellow asterisk in J) and thin incisor DE (yellow arrows) in *Phospho1*$^{-/-}$ mouse incisors. (**K–N**) Histology reveals an altered mantle dentin (MD) layer of *Phospho1*$^{-/-}$ versus WT control mice, including increased width and globular appearance. AB, alveolar bone; M1, first molar; M2, second molar; PDL, periodontal ligament; SAG, sagittal plane.

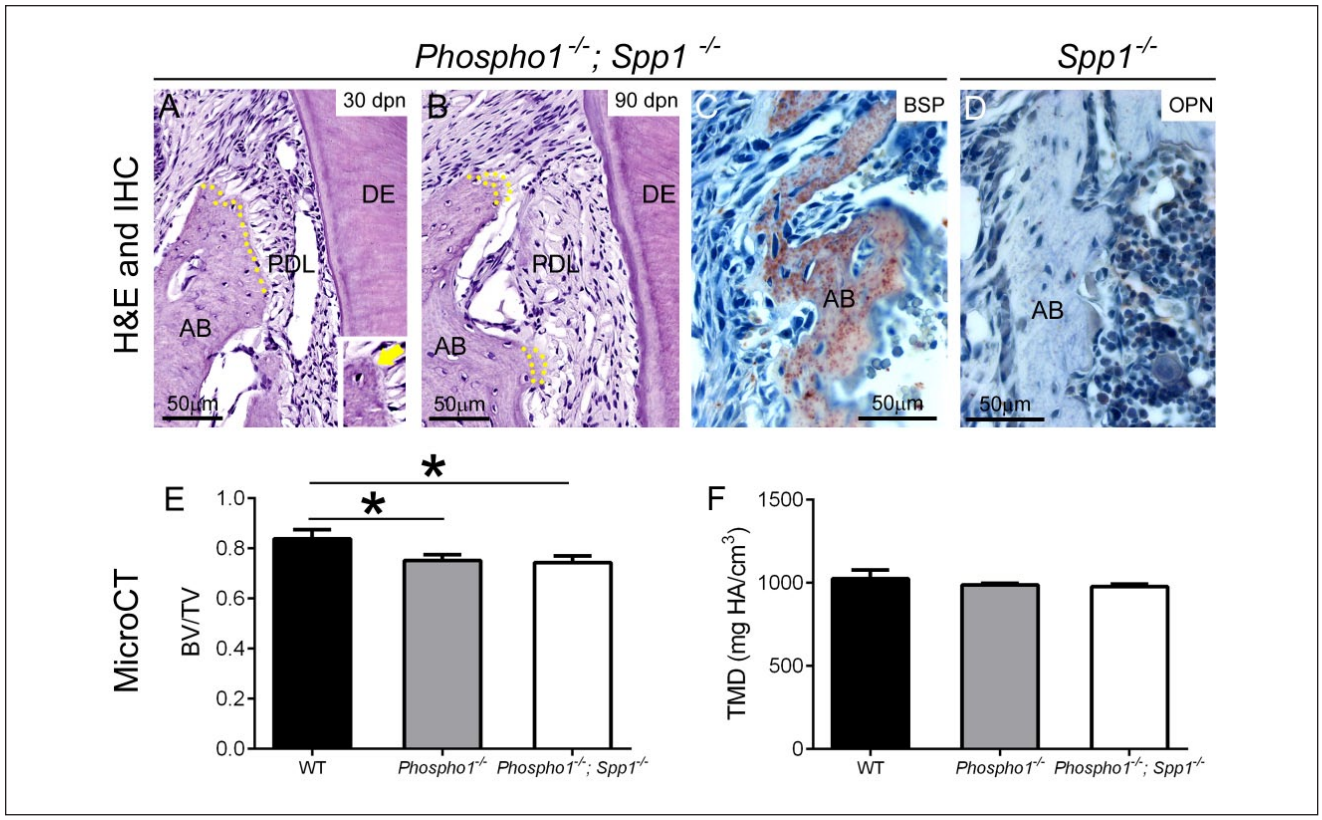


**Appendix Figure 5.** Ablation of osteopontin (OPN) does not reverse alveolar bone defects from loss of Orphan Phosphatase 1 (PHOSPHO1). (**A, B**) Observation of hematoxylin and eosin (H&E)–stained histological sections of first mandibular molar regions of *Phospho1*$^{-/-}$; *Spp1*$^{-/-}$ double-deficient mice at 30 and 90 d postnatal (dpn) reveals mineralization delays and osteoid accumulation at the alveolar bone (AB) crest (indicated by yellow dotted outlines), similar to *Phospho1*$^{-/-}$ mice (see Fig. 4). (**C**) OPN immunostaining in *Phospho1*$^{-/-}$; *Spp1*$^{-/-}$ double-deficient mice identifies a globular deposition pattern similar to *Phospho1*$^{-/-}$ mice (see Fig. 4). (**D**) Lack of OPN immunostaining in AB confirms its loss in *Phospho1*$^{-/-}$; *Spp1*$^{-/-}$ double-deficient mice. (**E, F**) Quantitative micro–computed tomography (micro-CT) analysis of AB reveals a statistically significant reduction (*$P < 0.05$) in bone volume fraction (BV/TV) (E) and a nonsignificant trend of decreased TMD (F) in *Phospho1*$^{-/-}$; *Spp1*$^{-/-}$ double-deficient mice compared with WT, with no significant difference or apparent improvement compared to *Phospho1*$^{-/-}$ mice. Micro-CT data for all dental tissues are summarized in the Appendix Table. DE, dentin; PDL, periodontal ligament.

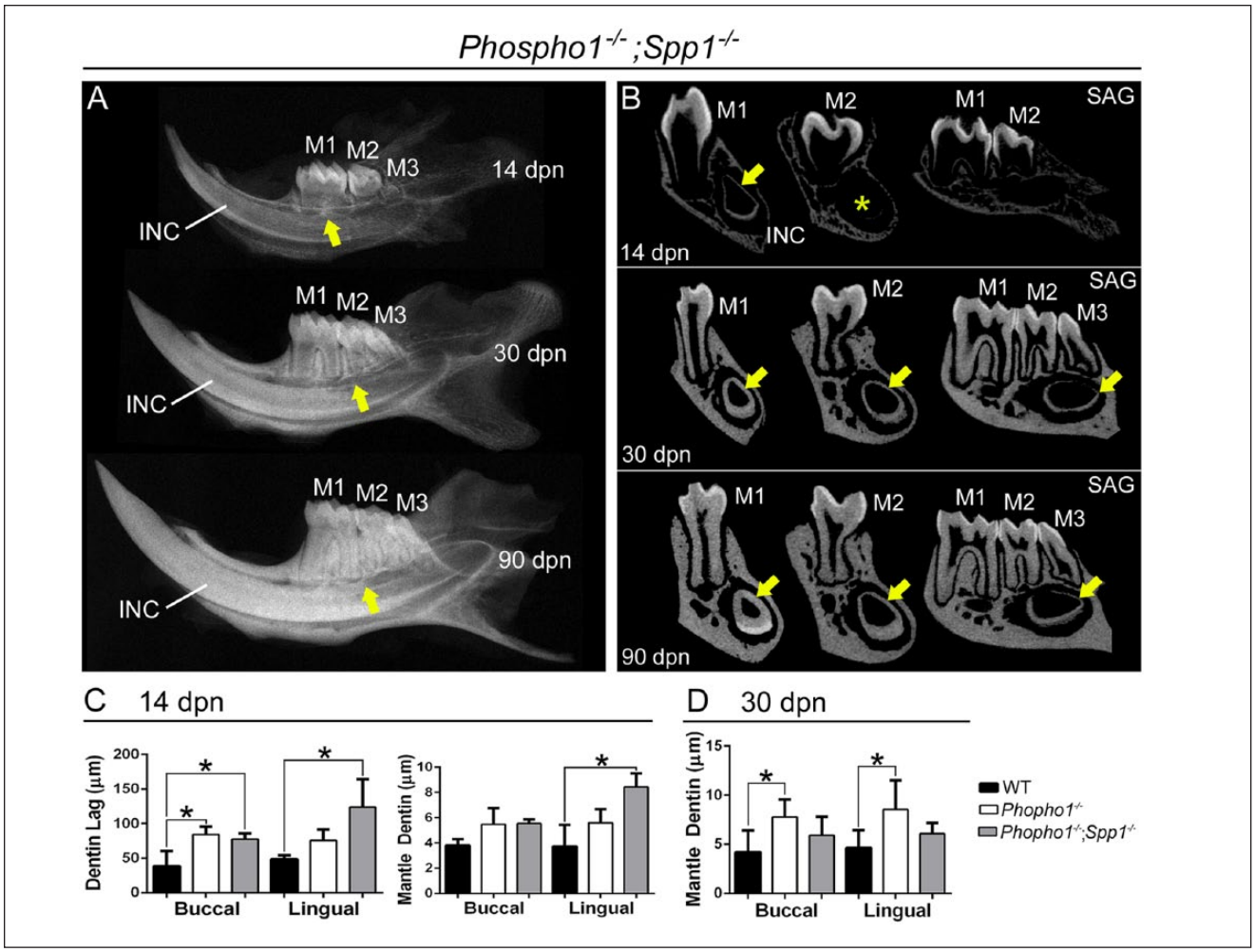


**Appendix Figure 6.** Ablation of osteopontin (OPN) does not reverse dentin defects from loss of Orphan Phosphatase 1 (PHOSPHO1). Dentin defects in *Phospho1*$^{-/-}$;*Spp1*$^{-/-}$ double-deficient mice are similar to those in *Phospho1*$^{-/-}$ mice (see Appendix Figs. 2 to 4 for comparison). (**A**) Radiography of the mandible at 14, 30, and 90 d postnatal (dpn), indicates consistently delayed dentin (DE) mineralization of the *Phospho1*$^{-/-}$;*Spp1*$^{-/-}$mouse incisor (INC), where the incisor lingual (root) aspect initiates beneath the first or second molar (M1 or M2, respectively; yellow arrow). (**B**) Micro–computed tomography analysis at 14, 30, and 90 dpn indicates delayed DE mineralization (yellow asterisk at 14 dpn) and thin incisor DE (yellow arrows at 14, 30, and 90 dpn) in *Phospho1*$^{-/-}$;*Spp1*$^{-/-}$mouse INC. (**C**) Histomorphometry conducted on 14 dpn hematoxylin and eosin (H&E)–stained sections confirms a significantly larger (*$P < 0.05$) lag in *Phospho1*$^{-/-}$;*Spp1*$^{-/-}$molar dentin mineralization (similar to *Phospho1*$^{-/-}$ mice) compared with the wild type (WT), and a trend for increased mantle dentin thickness in both *Phospho1*$^{-/-}$;*Spp1*$^{-/-}$ and *Phospho1*$^{-/-}$ mice. (**D**) Histomorphometry conducted on 30 dpn H&E-stained sections confirms a trend for increased mantle dentin thickness in both *Phospho1*$^{-/-}$;*Spp1*$^{-/-}$ and *Phospho1*$^{-/-}$ mice. M3, third molar; SAG, sagittal plane.

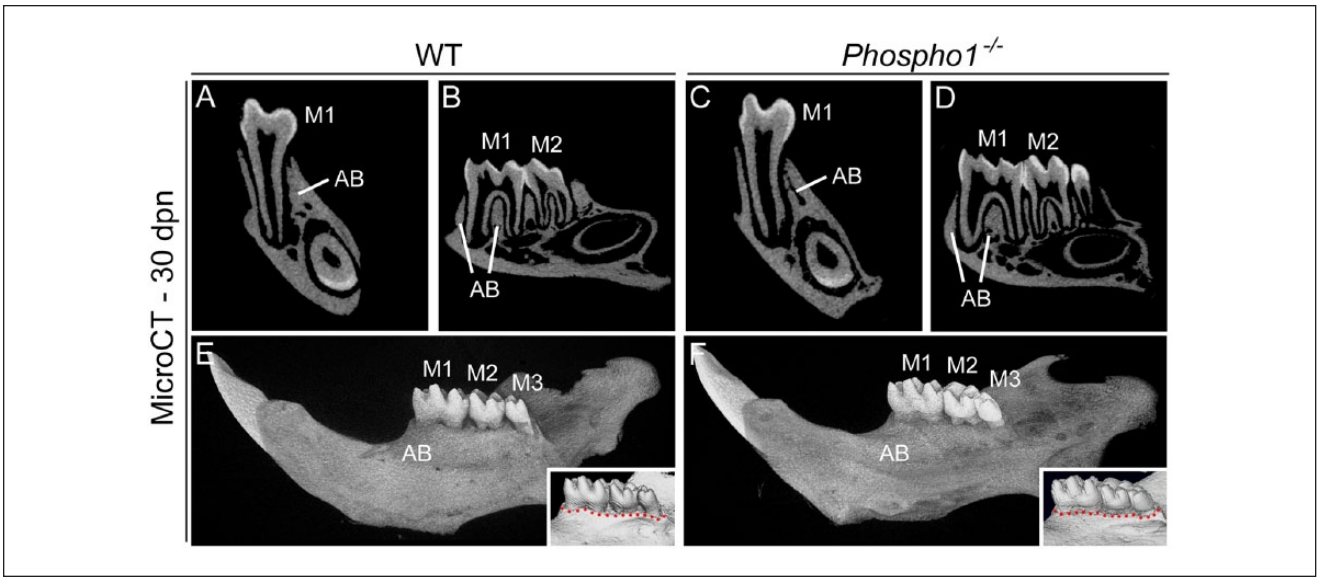


**Appendix Figure 7.** Loss of Orphan Phosphatase 1 (PHOSPHO1) does not alter periodontal parameters at 30 d postnatal (dpn). (**A–F**) Analysis of micro–computed tomography 2-dimensional cross-sections and 3-dimensional renderings at 30 dpn does not identify any measurable alveolar bone (AB) loss surrounding the mandibular molars (M1, M2, and M3). Insets in E and F show similar alveolar crest height (red dotted line) in *Phospho1*$^{-/-}$ and wild-type (WT) mice.

**Appendix Table.** Micro–Computed Tomography Analysis of Dental Tissues in *Phospho1*$^{-/-}$ Versus WT Controls.

| Tissue | WT | *Phospho1*$^{-/-}$ | *Phospho1*$^{-/-}$*; Spp1*$^{-/-}$ |
|---|---|---|---|
| Alveolar bone | | | |
| TV ($\mu m^3$) | 145.3 ± 19.8 | 138.8 ± 33.0 | 123.62 ± 16.6 |
| BV ($\mu m^3$) | 122.0 ± 19.9 | 104.9 ± 27.1 | 91.9 ± 14.0 |
| BV/TV (%) | 83.77 ± 0.04 | 75.23 ± 2.28[a] | 74.26 ± 2.69[a] |
| TMD (mg HA/$cm^3$) | 1,025 ± 51 | 988 ± 9 | 977 ± 16 |
| Dentin | | | |
| TV ($\mu m^3$) | 405.3 ± 38.2 | 361.5 ± 14.2 | 367.6 ± 22.3 |
| BV ($\mu m^3$) | 353.3 ± 24.4 | 328.9 ± 14.6 | 326.1 ± 15.1 |
| BV/TV (%) | 87.37 ± 3.73 | 90.96 ± 0.90 | 88.78 ± 2.03 |
| TMD (mg HA/$cm^3$) | 1,248 ± 55 | 1,231 ± 27 | 1,228 ± 7 |
| Enamel | | | |
| TV ($\mu m^3$) | 208.4 ± 8.2 | 194.2 ± 6.2 | 188.2 ± 11.2 |
| BV ($\mu m^3$) | 204.6 ± 8.8 | 191.0 ± 5.9 | 185.0 ± 11.0 |
| BV/TV (%) | 98.19 ± 0.54 | 98.34 ± 0.33 | 98.28 ± 0.26 |
| TMD (mg HA/$cm^3$) | 1,909 ± 63 | 1,860 ± 11 | 1,886 ± 22 |
| Thickness ($\mu m$) | 63.4 ± 6.2 | 60.6 ± 1.8 | 60.0 ± 1.9 |

Tissues were compared at 30 d postnatal. Values for WT, *Phospho1*$^{-/-}$, and *Phospho1*$^{-/-}$*; Spp1*$^{-/-}$ ($n$ = 5 each) samples are shown as means ± SD. No differences were found between WT and *Spp1*$^{-/-}$; therefore, the latter sample values were not included with this data table.
BV, bone volume; HA, hydroxyapatite; TMD, tissue mineral density; TV, tissue volume; WT, wild type.
[a]$P < 0.05$ (by independent-samples $t$ test, compared with WT).